AMERICAN SOCIETY FOR MICROBIOLOGY | Molecular and Cellular Biology®

RESEARCH ARTICLE

Alternative Splicing of the Aryl Hydrocarbon Receptor Nuclear Translocator (ARNT) Is Regulated by RBFOX2 in Lymphoid Malignancies

Amy M. Cooper,[a,b] Curtis A. Nutter,[c*] Muge N. Kuyumcu-Martinez,[c,d] Casey W. Wright[a,b]

[a]Department of Pharmacology and Toxicology, The University of Texas Medical Branch, Galveston, Texas, USA
[b]Toxicology Training Program, The University of Texas Medical Branch, Galveston, Texas, USA
[c]Department of Biochemistry and Molecular Biology, The University of Texas Medical Branch, Galveston, Texas, USA
[d]Department of Neuroscience, Cell Biology and Anatomy, The University of Texas Medical Branch, Galveston, Texas, USA

ABSTRACT Aberrant alternative splicing (AS) of pre-mRNAs promotes the development and proliferation of cancerous cells. Accordingly, we had previously observed higher levels of the aryl hydrocarbon receptor nuclear translocator (ARNT) spliced variant isoform 1 in human lymphoid malignancies compared to that in normal lymphoid cells, which is a consequence of increased inclusion of alternative exon 5. ARNT is a transcription factor that has been implicated in the survival of various cancers. Notably, we found that ARNT isoform 1 promoted the growth and survival of lymphoid malignancies, but the regulatory mechanism controlling *ARNT* AS is unclear. Here, we report *cis*- and *trans*-regulatory elements which are important for the inclusion of *ARNT* exon 5. Specifically, we identified recognition motifs for the RNA-binding protein RBFOX2, which are required for RBFOX2-mediated exon 5 inclusion. RBFOX2 upregulation was observed in lymphoid malignancies, correlating with the observed increase in *ARNT* exon 5 inclusion. Moreover, suppression of RBFOX2 significantly reduced ARNT isoform 1 levels and cell growth. These observations reveal RBFOX2 as a critical regulator of *ARNT* AS in lymphoid malignancies and suggest that blocking the *ARNT*-specific RBFOX2 motifs to decrease ARNT isoform 1 levels is a viable option for targeting the growth of lymphoid malignancies.

KEYWORDS ARNT, RBFOX2, alternative splicing, lymphoid malignancies

The aryl hydrocarbon receptor nuclear translocator (ARNT), also known as hypoxia-inducible factor-1β (HIF-1β), is a member of the basic-helix-loop-helix/Per-ARNT-Sim superfamily of transcription factors, which act as sensors of environmental or physiological insults and are associated with the initiation and progression of cancerous cells (1–3). Specifically, ARNT has been implicated in chemotherapeutic resistance in cancer cells through the depletion of reactive oxygen species (4–7). Conversely, ARNT has also been reported to hinder tumor migration and invasion (8). These observations suggest that targeting ARNT has potential for treating drug-resistant cancer but could lead to undesirable effects such as increased metastasis. Thus, reconciling these divergent functions of ARNT in cancer pathogenesis will be critical for developing ARNT-based therapeutic strategies. In consideration of the different roles ascribed to ARNT, it is important to note that *ARNT* is alternatively spliced to produce two main isoforms, ARNT isoform 1 and ARNT isoform 3, which differ by the inclusion or exclusion of exon 5, respectively (9). Moreover, we have previously reported that increased levels of ARNT isoform 1 in diverse lymphoid malignancies correspond to better growth and higher thresholds for killing with doxorubicin (10). Interestingly, suppression of total ARNT (i.e., both isoforms) conveyed a greater growth rate compared to that of cells

Address correspondence to Casey W. Wright, cawright@utmb.edu.

*Present address: Curtis A. Nutter, Department of Genetics and Microbiology, University of Florida, Gainesville, Florida, USA.

The authors declare no conflict of interest.

Received 28 October 2021
Returned for modification 20 December 2021
Accepted 17 March 2022
Published 11 April 2022

with high ARNT isoform 1 levels (10). Thus, targeting the specific ARNT isoforms may lead to a more promising therapeutic approach. While we have illuminated the differential roles of the ARNT isoforms in regulating the growth and survival of lymphoid malignancies, there is a lack of understanding on the mechanism(s) controlling *ARNT* alternative splicing (AS).

AS is regulated by *trans*-acting factors (RNA-binding proteins) binding to *cis*-regulatory sequences (RNA-binding motifs), which in turn mediate alternative splicing, and yields multiple mature RNA isoforms from the same pre-mRNA molecule (11). AS is essential for maintaining many physiological processes, but its dysregulation can contribute to cancer pathogenesis (12, 13). In fact, the Cancer Genome Atlas reports that malignant tissues display approximately 30% more alternative splicing events compared to non-malignant tissues (14), which have been attributed to mutations in, and/or expression levels of, genes encoding splicing regulators (15, 16). For instance, members of the RNA-binding Fox (RBFOX) protein family, consisting of RBFOX1, RBFOX2, and RBFOX3, are master regulators of AS due to their interactions with the intronic GCAUG sequence motifs which flank alternative exons in pre-mRNA (17, 18). Although each family member of the RBFOX family recognizes the same RNA motif, they differ in their tissue specific expression patterns. RBFOX1 is predominately expressed in the brain, heart, and ovaries, whereas RBFOX3 is expressed almost exclusively in the brain (19–23). RBFOX2 is more widely expressed than other family members and is upregulated in diverse cancers (24–26). Specifically, RBFOX2 contributes to cellular invasion, is highly expressed in cells undergoing epithelial-mesenchymal transition, and appears to be important for maintaining a mesenchymal phenotype (27–29). In addition, RBFOX2 is highly expressed in various B and T cell malignancies (30).

Given our observations of ARNT isoform 1-dependent proliferation of lymphoid malignancies, and the possible correlation with higher RBFOX2 expression in malignant cells, we hypothesized that RBFOX2 regulates *ARNT* AS. In this study, we identified RBFOX2 binding motifs in *ARNT* introns 4 and 5, which flank exon 5. We demonstrate, using an *ARNT*-specific minigene, that RBFOX2 recognizes both a proximal and a distal motif in *ARNT* intron 5 to promote exon 5 inclusion. Overall, our data indicate that RBFOX2, an RNA-binding protein commonly upregulated in malignant cells, contributes to the aberrant AS of *ARNT* in lymphoid malignancies.

RESULTS

RBFOX2 binding sites in *ARNT* introns 4 and 5 correlate with RBFOX2-mediated *ARNT* exon 5 inclusion. To gain insight into the regulatory mechanism(s) controlling *ARNT* AS, we analyzed the intronic sequences flanking exon 5 for RNA binding motifs and observed multiple GCAUG motifs which are recognized by the RBFOX protein family (Fig. 1A). Next, we used RBFOX2-specific enhanced cross-linking and immunoprecipitation (eCLIP) data from K652 cells, a chronic myelogenous leukemia cell line, found within the Encyclopedia of DNA Elements (ENCODE) database. In alignment with the observed GCAUG motifs, we identified RBFOX2 binding peaks in *ARNT* introns 4 and 5, which flank exon 5 (Fig. 1B) (31). To determine whether RBFOX2 regulates *ARNT* AS, we depleted RBFOX2 in human embryonic kidney (HEK)293 cells. As a control, other RNA-binding proteins were also suppressed, including PTBP1/2 and CELF1, which do not display binding sites within *ARNT* introns 4 and 5. Notably, suppression of RBFOX2 significantly affected the inclusion of *ARNT* exon 5 (Fig. 1C), consistent with the presence of RBFOX2 binding sites in the introns flanking alternative exon 5; however, suppression of PTBP1/2 or CELF1 did not affect *ARNT* AS. We further assessed RBFOX2-mediated regulation of *ARNT* AS during murine heart development, because RBFOX2 protein levels are low at birth but higher in adulthood (32). During murine heart development, inclusion of *ARNT* exon 5 correlated with expected RBFOX2 levels (Fig. 1D). Together, these observations from human cells and mouse tissue point to RBFOX2 as a critical regulator of *ARNT* AS.

RBFOX2 promotes *ARNT* exon 5 inclusion through recognition of *cis*-regulatory elements in *ARNT* intron 5. Both the upstream and downstream introns of *ARNT* exon 5 harbor multiple GCAUG motifs, and eCLIP validated RBFOX2 binding clusters within

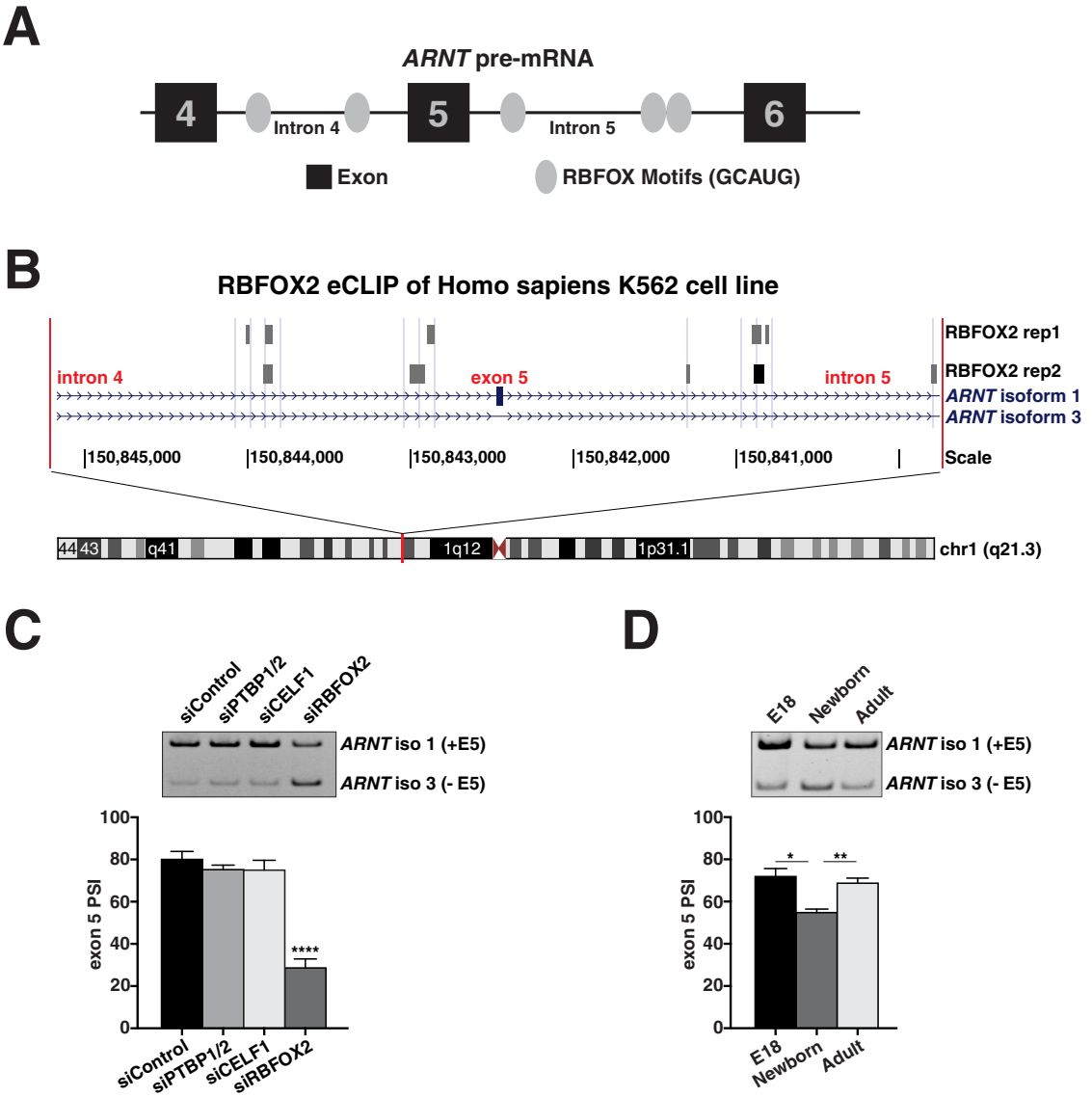

FIG 1 RBFOX2 binding sites in *ARNT* introns 4 and 5 correlate with RBFOX2-mediated *ARNT* exon 5 inclusion. (A) Schematic showing RBFOX2 binding motifs "GCAUG" in the upstream and downstream introns of *ARNT* exon 5. (B) RBFOX2 binding peaks in introns flanking *ARNT* exon 5 from two independent eCLIP experiments (rep1 and rep2), as found in the ENCODE database (GEO: GSE92030). (C) Representative reverse-transcription PCR (RT-PCR) analysis of *ARNT* AS in HEK293 cells after introduction of the indicated siRNAs (top), and combined densitometry analysis to determine percent spliced in (PSI) of three independent experiments performed in duplicate (bottom). (D) Representative RT-PCR analysis of *ARNT* AS in murine heart tissue at the indicated developmental stage (top), and combined densitometry analysis to determine PSI of $n = 3$ (E18 and Newborn) or $n = 4$ (Adult) (bottom). Data in graphs are presented as means ± standard error of the mean (SEM). E5 = exon 5. *P* values are derived using a two-tailed unpaired Student's *t* test. *, $P < 0.05$; **, $P < 0.01$; ****, $P < 0.0001$.

these regions. The position activity profile of RBFOX2 proteins, obtained through mechanism-based studies, identified that binding upstream from an exon promotes exclusion, whereas downstream binding promotes exon inclusion (18, 33). Thus, we focused on the GCAUG motifs in the downstream intron, given our observed RBFOX2-dependent inclusion of *ARNT* exon 5 (Fig. 1C and D). To map the probable RBFOX2 binding motifs necessary for exon 5 inclusion, we constructed an *ARNT* minigene splicing vector consisting of *ARNT* exon 5 and flanking introns. Next, we deleted the proximal RBFOX2-recognition motif (*ARNTΔp*), the distal motif (*ARNTΔd*), or both the proximal and distal motifs together (*ARNTΔpd*) (Fig. 2A). We then transfected the wild-type (WT) and the three mutant *ARNT* splicing vectors, with or without an *RBFOX2*-expressing plasmid, into HEK293T cells. As a

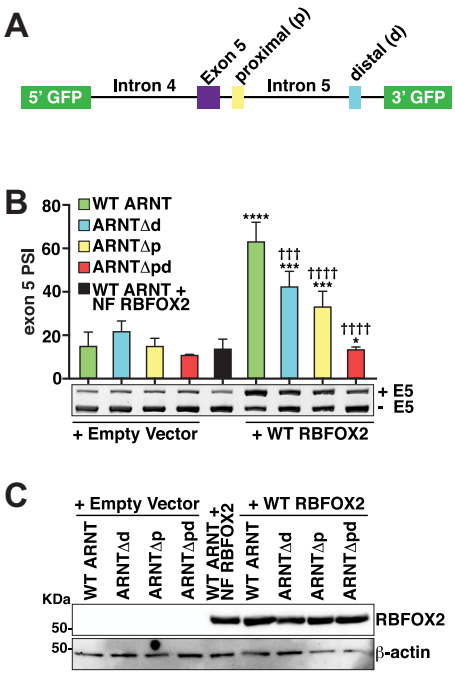

FIG 2 RBFOX2 promotes *ARNT* exon 5 inclusion through recognition of *cis*-regulatory elements in *ARNT* intron 5. (A) Schematic of *ARNT*-specific splicing vector with the indicated GCATG motifs that were targeted for deletion. (B) HEK293T cells were transfected with wild-type (WT) *ARNT* splicing vector or a GCATG deletion mutant *ARNT* splicing vector (*ARNTΔp*, *ARNTΔd*, or *ARNTΔpd*) plus empty vector control or WT RBFOX2. A nonfunctional (NF) RBFOX2 mutant was used as a negative control. Total RNA was isolated at 72 h posttransfection and analyzed by RT-PCR for splicing changes; a representative image is shown below the graph. The densitometry analysis to determine percent spliced in (PSI) results presented in the graph are means ± SEM of three independent experiments performed in triplicate. *P* values are derived using a two-tailed unpaired Student's *t* test. *, $P < 0.05$; ***, $P < 0.001$; ****, $P < 0.0001$ compared to empty vector control; †††, $P < 0.001$; ††††, $P < 0.0001$ compared to WT *ARNT* + WT *RBFOX2*. E5 = exon 5. (C) Immunoblot analysis of cells from panel B, showing equal levels of ectopically expressed FLAG-RBFOX2 between samples.

negative control, we transfected the WT *ARNT* splicing vector together with a nonfunctional (NF) *RBFOX2*-expressing plasmid which was mutated at the RNA recognition motif so that RBFOX2 could not bind to RNA targets. As expected, we observed that the cotransfection of the WT *ARNT* minigene with the *RBFOX2*-expressing plasmid promoted significant inclusion of exon 5, resulting in a percent spliced in (PSI) of 65% compared to 15% with an empty vector or NF *RBFOX2*-expressing plasmid (Fig. 2B and C). However, deletion of the proximal binding motif, *ARNTΔp*, in the presence of RBFOX2 resulted in a significant decrease in ARNT exon 5 inclusion (~30% PSI), compared to the WT *ARNT* splicing vector. Similarly, deletion of the distal binding motif, *ARNTΔd*, also significantly hindered RBFOX2-mediated inclusion of ARNT exon 5 (~20% PSI), compared to the WT *ARNT* splicing vector (Fig. 2B). Notably, deleting both RBFOX2 binding motifs, as in *ARNTΔpd*, resulted in a significant 50% decrease of exon 5 PSI compared to the WT *ARNT* splicing vector, suggesting that the function of RBFOX2 toward exon 5 inclusion is additive (Fig. 2B). In fact, the *ARNTΔpd* mutation brought exon 5 inclusion to background levels, suggesting that both the proximal and distal GCAUG motifs in *ARNT* intron 5 are essential for RBFOX2-mediated inclusion of *ARNT* exon 5 into the final mRNA.

RBFOX2 promotes the inclusion of *ARNT* exon 5, and higher ARNT isoform 1 levels, in lymphoid malignancies. To investigate whether a direct relationship exists between RBFOX2 and the increased ARNT isoform 1 levels that we previously observed in lymphoid malignancies (10), we first compared RBFOX2 expression between primary human T cells and two malignant human T cell lines: Karpas 299 cells, an anaplastic large cell lymphoma (ALCL) cell line; and Jurkat cells, an acute T cell leukemia cell line. Remarkably, *RBFOX2* expression was upregulated in the malignant T cells compared to

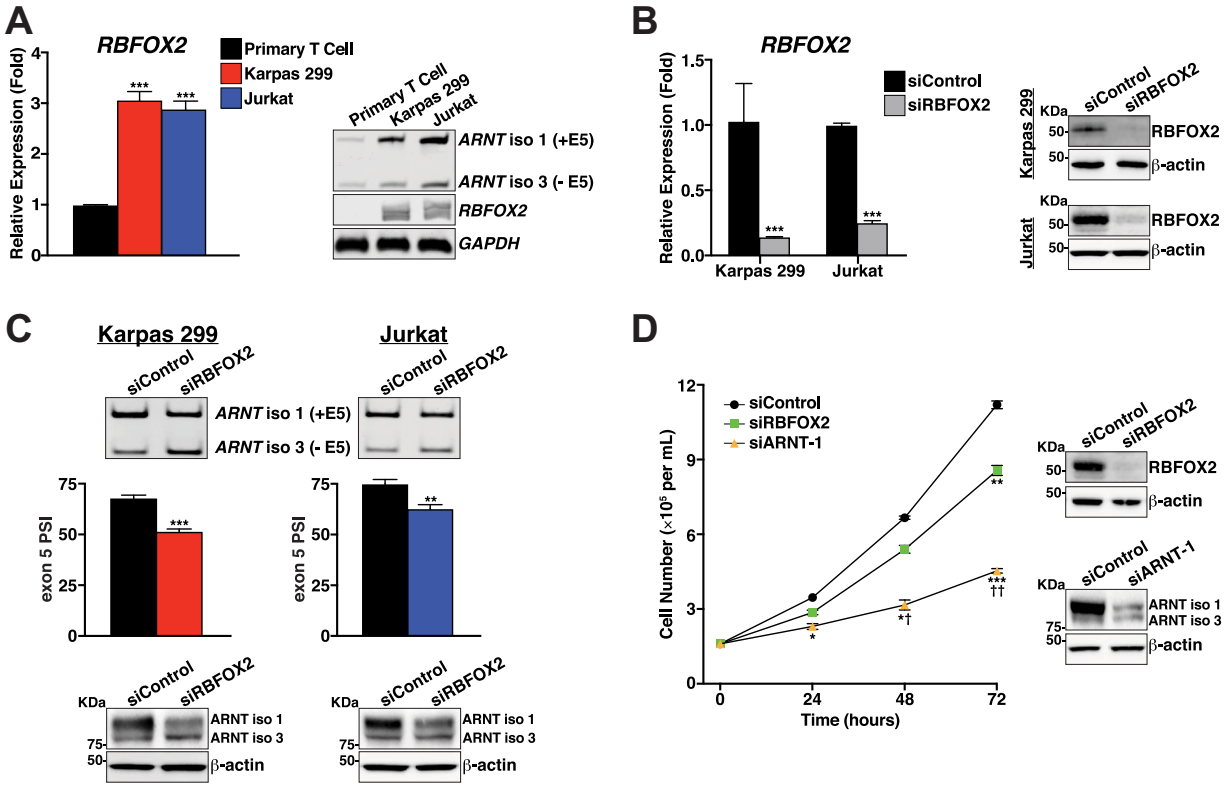

FIG 3 RBFOX2 promotes the inclusion of *ARNT* exon 5, and higher ARNT isoform 1 levels, for optimal growth of lymphoid malignancies. (A) RT-qPCR analysis of *RBFOX2* expression in primary T cells, Karpas 299 cells, and Jurkat cells (left), with representative RT-PCR images to show relative expression levels of *ARNT* and *RBFOX2* (right). (B) Validation of RNAi-mediated RBFOX2 suppression by RT-qPCR analysis (left) and immunoblotting with antibodies against RBFOX2 and β-actin (right), in Karpas 299 and Jurkat cells. RT-qPCR data are means ± SEM of three independent experiments performed in triplicate. *P* values are derived using a two-tailed unpaired Student's *t* test. **, $P < 0.01$; ***, $P < 0.001$. (C) Representative RT-PCR analysis of *ARNT* AS in Karpas 299 and Jurkat cells after introduction of the indicated siRNAs (top), percent spliced in (PSI) as determined by combined densitometry analysis (data are means ± SEM of three independent experiments) (middle), and immunoblot analysis using antibodies against ARNT and β-actin (bottom). E5 = exon 5. (D) Twenty-four hours post-electroporation with siControl, siRBFOX2, or siARNT-1, Karpas 299 cells were normalized to 1.7×10^5 cells/mL and counted every 24 h for a total of 72 h (left). *P* values are derived using two-way analysis of variance. *, $P < 0.05$; **, $P < 0.01$; ***, $P < 0.001$ compared to siControl. †, $P < 0.05$; ††, $P < 0.01$ compared to siRBFOX2. Immunoblot analysis was performed at 48 h posttransfection using antibodies against RBFOX2, ARNT, and β-actin (right).

that in primary T cells, as assessed by real-time quantitative PCR (RT-qPCR) and reverse-transcription PCR (RT-PCR) analysis (Fig. 3A). Next, we suppressed RBFOX2 in both malignant T cells and observed a significant decrease in *ARNT* exon 5 inclusion at the transcription and protein levels (Fig. 3B and C). Importantly, the loss of RBFOX2 significantly reduced the growth of Karpas 299 cells in proportion to the loss of ARNT isoform 1 (Fig. 3D). These observations demonstrate that RBFOX2 is upregulated in malignant T cells and acts as a positive mediator of *ARNT* exon 5 inclusion, resulting in the predominant generation of ARNT isoform 1, which imparts an increased growth advantage.

DISCUSSION

Aberrant AS plays a significant role in promoting tumorigenesis and proliferation of cancerous cells. The transcription factor ARNT has been implicated in the development of cancerous cells (34, 35), and we have previously shown that, compared to normal lymphoid cells, ARNT is alternatively spliced in lymphoid malignancies so that ARNT isoform 1 is the predominant isoform (10, 34, 35). Subsequently, ARNT isoform 1 promotes the growth of the lymphoid cancers and resistance to the chemotherapeutic drug doxorubicin (10). In the current study, our goal was to elucidate the regulatory factor(s) responsible for promoting *ARNT* AS. Accordingly, by utilizing available eCLIP

data from the ENCODE database, analyzing the *cis*-regulatory motifs in the intronic regions flanking *ARNT* exon 5, and suppressing certain RNA-binding proteins via RNA interference (RNAi), we were able to identify RBFOX2 as a key regulator of *ARNT* AS. Moreover, we confirmed that RBFOX2 is upregulated in human T cell-derived ALCL and leukemia cells and promotes the inclusion of *ARNT* exon 5 through recognition of proximal and distal *cis*-regulatory motifs in *ARNT* intron 5. Combined, our data support a cell-proliferative role for RBFOX2 through the promotion of increased ARNT isoform 1 levels.

Commonly, AS studies focus within the 500-nucleotide intronic regions flanking alternative exons to analyze the *cis*-regulatory motifs and *trans*-acting factors which bind to these sequences (36). However, studies have shown that RNA-binding proteins have important binding sites located much further beyond this arbitrary 500-nucleotide boundary (37) and are recruited closer to the alternative exon through an "RNA bridge" to enhance spliceosome activity (38). RNA bridges are created through RNA secondary-structure changes which dramatically shorten the distance of a distal *cis*-regulatory motif to its target exon. Thus, we predict that the proximal and distal GCAUG motifs downstream from *ARNT* exon 5 are brought into proximity to allow for optimal RBFOX2-mediated *ARNT* exon 5 inclusion, possibly through an RNA bridge, as previously demonstrated for RBFOX2 (38). Our data further suggest that analyzing *cis*-regulatory sequences outside of the commonly used 500-nucleotide intronic regions is an important consideration when investigating exon usage regulation in AS studies.

Although this study focused specifically on RBFOX2 regulation of *ARNT* AS in lymphoid malignancies, RBFOX2 is known to be upregulated in many other cancer cell types, such as breast and ovarian cancers (29). Interestingly, RBFOX2 expression is associated with promoting the progression of epithelial to mesenchymal cell transition by regulating the AS of genes important for tissue invasion (27, 29). Notably, *ARNT* AS was found to be more affected in mesenchymal tissues versus epithelial tissues, correlating with RBFOX2 expression levels (29). Thus, the ARNT isoforms may play a pivotal role in regulating the growth and invasion of non-lymphoid cancerous cells. Together, our observations suggest that targeting the splicing of *ARNT* by blocking RBFOX2 from binding to the *ARNT* pre-mRNA provides a more specific strategy for cancer therapeutics.

MATERIALS AND METHODS

Cell culture. HEK293 and HEK293T cells were cultured in Dulbecco's Modified Eagle medium (DMEM; Corning, 15-018-CV) complete with 10% fetal bovine serum (FBS; Atlanta Biologicals, S11550) and 2 mM GlutaMAX (GIBCO, 35050-061) at 37°C, 5% CO_2. Karpas 299 and Jurkat cells were cultured in RPMI 1640 medium (Corning, 15-041-CV) complete with 10% FBS and 2 mM GlutaMAX at 37°C, 5% CO_2.

Mice. All animal experiments were approved by the University of Texas Medical Branch Institutional Animal Care and Use Committee (protocol no. 1101001) and were conducted in accordance with NIH guidelines. For analysis of *ARNT* AS during development, C57BL6 (Jackson Laboratory) mice were purchased and timed matings were conducted. At embryonic day 18 (E18), the day of birth (Newborn), and 6 months of age (Adult), mice were terminated, and heart tissue was collected for RNA extraction using TRIzol Reagent (Invitrogen, 15596).

Plasmids. The p3×FLAG-RBFOX2 plasmid has been previously described (39). The control empty vector was the p3×FLAG plasmid (Millipore Sigma, E7408). The ARNT minigene splicing reporter was constructed as follows: pcDNA5-GFP-IL7R splicing reporter (40) was digested with ApaI and BamHI (New England BioLabs [NEB]) and purified with a PCR purification kit (Qiagen). The genomic sequence of *ARNT* exon 5 and the upstream and downstream introns were ligated into the vector using T4 DNA ligase (NEB). Site-directed mutagenesis was performed to delete the indicated GCATG motifs using a Quikchange Lightning mutagenesis kit (Agilent, 210518). Primers were designed using the Agilent primer design tool and the sequences used were as follows: *ARNTΔp*, sense 5′-GTA GGA GAA CAG TGT CTT TTG AAG CAG ATG ATG CTG CT-3′ and nonsense 5′-AG CAG CAT CAT CTG CTT CAA AAG ACA CTG TTC TCC TAC-3′; *ARNTΔd*, sense 5′-GAG TAG AAG CAG CTC CTT GAG GCA TCC-3′ and nonsense 5′-GGA TGC CTC AAG GAG CTG CTT CTA CTC-3′. Resultant deletions were confirmed by DNA sequencing.

Transfections. HEK293 cells were transfected with 10 μM Control scrambled siRNA (Invitrogen AM4611), a pool of 10 μM CELF1-targeting siRNAs (Invitrogen siRNA ID no. s168616 and s168617), 10 μM human PTBP1/PTBP2-targeting siRNAs (Qiagen, SI02649206 and SI04255146), or a RBFOX2-specific siRNA (Invitrogen siRNA IDnumber s96620), using Lipofectamine RNAiMAX (Invitrogen, 13778100), and were harvested 72 h later. HEK293T cells were transfected with 100 ng *ARNT*

minigene splicing vector, and 250 ng of either empty vector or FLAG-tagged RBFOX2, using a standard calcium-phosphate transfection protocol. DMEM was replaced 7 h later, and cells were harvested after 72 h. Karpas 299 and Jurkat cells were transfected with 4 μM RBFOX2-targeting siRNA (5′-GUU CGU AAC UUU CGA GAA U-3′; Millipore Sigma), 4 μM Control scrambled siRNA (5′-CAU GCC UUG CUU UAC GCA U-3′; Millipore Sigma), or 4 μM ARNT isoform 1-targeting siRNA (10) using a Bio-Rad Gene Pulser Xcell electroporator set on infinite resistance, 950 microfarads, and 300 V for Karpas 299 cells or 250 V for Jurkat cells. Sixteen hours posttransfection, dead cells were removed with Ficoll-Paque (GE Healthcare, 17-1440-02) by centrifugation at 400 $\times$ *g* for 20 min. The live cell layer was collected, washed with phosphate-buffered saline, resuspended in RPMI medium at 0.5 $\times$ 10^6 cells/mL, and propagated for an additional 32 h.

RT-PCR analysis of RNA from human cell culture. Total RNA was extracted using a QIAshredder (Qiagen, 79656) and RNeasy columns (Qiagen, 74104). Two μg of total RNA was converted to cDNA using the iScript cDNA synthesis kit (Bio-Rad, 1706691). PCR primers were designed to detect inclusion/exclusion (185-bp product and 140-bp product, respectively) of human *ARNT* exon 5: forward 5′-GCG ATG ATG ACC AGA TGT GT-3′ and reverse 5′-GGC CAT GCG TAA GAT GGT TA-3′. The PCR (20 μL total) included 5 μL of cDNA, 25 μM dNTPs, and 100 ng of each *ARNT*-specific forward and reverse primer with Biolase *Taq* polymerase (Bioline BIO-21042). PCR conditions for each reaction were as follows: 95°C, 45 sec; 59°C, 45 sec; 72°C, 1 min for 25 cycles. PCR products were resolved on 5% non-denaturing polyacrylamide gels and stained with ethidium bromide. The bands were imaged using the ChemiDoc MP Imaging system (Bio-Rad). Unsaturated band intensities were quantified after normalizing the ethidium staining to the size of the included and excluded bands, and percent exon inclusion was calculated (i.e., percent spliced in [PSI]) using Image Lab software (Bio-Rad) with the following equation: PSI = ([exon inclusion band]/[exon inclusion band + exon exclusion band]*100).

RT-PCR analysis of RNA from mouse heart tissue. One μg of total RNA was incubated with 125 ng of oligo(dT) primer at 65°C for 10 min followed by cDNA synthesis using AMV reverse transcriptase (20 units/μg; Life Biosciences, AMV 007-1) in the presence of 10 μM dNTPs (20-μL reaction) at 42°C for 1 h. PCR primers were designed to detect inclusion/exclusion (221-bp product versus 176-bp product, respectively) of murine *ARNT* exon 5: forward 5′-GCG ATG ATG ACC AGA TGT GT-3′ and reverse 5′-GGC CAT GCG TAA GAT GGT TA-3′. The PCR (20 μL total) included 5 μL of cDNA, 25 μM dNTPs, 100 ng of each *ARNT*-specific forward and reverse primer, and Biolase *Taq* polymerase (Bioline BIO-21042). PCR conditions for each reaction were as follows: 94°C, 45 sec; 59°C, 45 sec; 72°C, 1 min for 25 cycles. PCR products were resolved on 5% non-denaturing polyacrylamide gels and stained with ethidium bromide. The DNA bands were imaged and analyzed as described above.

Real-time quantitative PCR analysis and cell growth assay. For this analysis, 300 ng of total RNA was converted to cDNA using the iScript cDNA synthesis kit (Bio-Rad, 1706691). The CFX96 Real Time System (Bio-Rad) was used to perform quantitative PCR (qPCR). The qPCR (20 μL total) included 1 μL of cDNA, SsoAdvanced Universal Probes Supermix (Bio-Rad, 1725284), and the *Homo sapiens* primer-probe assay *RBFOX2* (Bio-Rad, qHsa CIP0027070) or *GAPDH* (Bio-Rad, qHsa CEP0041396) as the internal reference gene used to determine fold changes with the threshold cycle (ΔC_T) method. The cell growth assay was performed as previously described (10).

Antibodies and immunoblot analysis. Whole-cell lysates from HEK293T, Karpas 299, and Jurkat cells were extracted by incubating cells with 1 $\times$ radioimmunoprecipitation assay (RIPA) lysis buffer (Cell Signaling, 9806S) complete with phosphatase inhibitor cocktail 2 (Millipore Sigma, P5726), phosphatase inhibitor cocktail 3 (Millipore Sigma, P0044), complete mini protease inhibitor tablets (Roche, 11836170001), and 50 mM sodium fluoride (Millipore Sigma, S1504-110G) on ice for 20 min. Protein samples were normalized using the Bradford assay, resolved on NuPAGE 4 to 12% Bis-Tris Gels (Invitrogen, NP0322BOX), and transferred onto nitrocellulose membranes (Bio-Rad, 1620215). Membranes were blocked with 1% Casein Blocker (Bio-Rad, 1610782) supplemented with 0.1% Tween 20. Membranes were incubated with the indicated antibodies, washed 4 times with Tris-buffered saline supplemented with 0.1% Tween 20, incubated with the relevant horseradish peroxidase (HRP)-conjugated secondary antibodies (GE Healthcare, Mouse-NA931 or Rabbit-NA934), and then washed 4 more times. Lastly, ECL substrate (Bio-Rad, 170-5060) was added to the membrane for 5 min and HRP activity was imaged on the ChemiDoc MP Imaging System (Bio-Rad). Antibodies used are as follows: ARNT (BD, 611079), RBFOX2 (Bethyl Laboratories, A300-864A), and β-actin (Millipore Sigma, A5316).

Statistical analysis. All data were graphed as mean $\pm$ standard error of the mean (SEM) and repeated at least three times unless otherwise indicated. Statistical differences between two individual groups were assessed by performing a two-tailed unpaired Student's *t* test using Prism software. Statistical differences between multiple groups were assessed by performing a two-way analysis of variance with Šídák's multiple-comparison test.

ACKNOWLEDGMENTS

This work was supported by grants from the National Institutes of Health/National Institute of Environmental Health Sciences, no. R01ES025809 (to C.W.W.) and T32ES007254 (to A.M.C.); Cancer Prevention and Research Institute of Texas no. RP190556 (to C.W.W. and M.N.K-M.); National Institutes of Health/National Heart Lung Blood Institute no. 1R01HL135031, UTMB John Sealy Memorial Endowment Pilot Award,

Additional Ventures Single Ventricle Research Fund no. 4873, and American Heart Association no. 20TPA35490206 (to M.N.K-M).

REFERENCES

1. Bersten DC, Sullivan AE, Peet DJ, Whitelaw ML. 2013. bHLH-PAS proteins in cancer. Nat Rev Cancer 13:827–841. https://doi.org/10.1038/nrc3621.
2. Kewley RJ, Whitelaw ML, Chapman-Smith A. 2004. The mammalian basic helix-loop-helix/PAS family of transcriptional regulators. Int J Biochem Cell Biol 36:189–204. https://doi.org/10.1016/S1357-2725(03)00211-5.
3. McIntosh BE, Hogenesch JB, Bradfield CA. 2010. Mammalian Per-Arnt-Sim proteins in environmental adaptation. Annu Rev Physiol 72:625–645. https://doi.org/10.1146/annurev-physiol-021909-135922.
4. Gu C, Gonzalez J, Zhang T, Kamel-Reid S, Wells RA. 2013. The aryl hydrocarbon receptor nuclear translocator (ARNT) modulates the antioxidant response in AML cells. Leuk Res 37:1750–1756. https://doi.org/10.1016/j.leukres.2013.10.010.
5. Hassen W, Kassambara A, Reme T, Sahota S, Seckinger A, Vincent L, Cartron G, Moreaux J, Hose D, Klein B. 2015. Drug metabolism and clearance system in tumor cells of patients with multiple myeloma. Oncotarget 6:6431–6447. https://doi.org/10.18632/oncotarget.3237.
6. Shi S, Yoon DY, Hodge-Bell KC, Bebenek IG, Whitekus MJ, Zhang R, Cochran AJ, Huerta-Yepez S, Yim S-H, Gonzalez FJ, Jaiswal AK, Hankinson O. 2009. The aryl hydrocarbon receptor nuclear translocator (Arnt) is required for tumor initiation by benzo[a]pyrene. Carcinogenesis 30:1957–1961. https://doi.org/10.1093/carcin/bgp201.
7. Shieh J-M, Shen C-J, Chang W-C, Cheng H-C, Chan Y-Y, Huang W-C, Chang W-C, Chen B-K. 2014. An increase in reactive oxygen species by deregulation of ARNT enhances chemotherapeutic drug-induced cancer cell death. PLoS One 9:e99242. https://doi.org/10.1371/journal.pone.0099242.
8. Huang C-R, Lee C-T, Chang K-Y, Chang W-C, Liu Y-W, Lee J-C, Chen B-K. 2015. Down-regulation of ARNT promotes cancer metastasis by activating the fibronectin/integrin β1/FAK axis. Oncotarget 6:11530–11546. https://doi.org/10.18632/oncotarget.3448.
9. Hoffman EC, Reyes H, Chu F-F, Sander F, Conley LH, Brooks BA, Hankinson O. 1991. Cloning of a factor required for activity of the Ah (dioxin) receptor. Science 252:954–958. https://doi.org/10.1126/science.1852076.
10. Gardella KA, Muro I, Fang G, Sarkar K, Mendez O, Wright CW. 2016. Aryl hydrocarbon receptor nuclear translocator (ARNT) isoforms control lymphoid cancer cell proliferation through differentially regulating tumor suppressor p53 activity. Oncotarget 7:10710–10722. https://doi.org/10.18632/oncotarget.7539.
11. Black DL. 2003. Mechanisms of alternative pre-messenger RNA splicing. Annu Rev Biochem 72:291–336. https://doi.org/10.1146/annurev.biochem.72.121801.161720.
12. Climente-González H, Porta-Pardo E, Godzik A, Eyras E. 2017. The functional impact of alternative splicing in cancer. Cell Rep 20:2215–2226. https://doi.org/10.1016/j.celrep.2017.08.012.
13. Dvinge H, Bradley RK. 2015. Widespread intron retention diversifies most cancer transcriptomes. Genome Med 7:45. https://doi.org/10.1186/s13073-015-0168-9.
14. Kahles A, Lehmann K-V, Toussaint NC, Hüser M, Stark SG, Sachsenberg T, Stegle O, Kohlbacher O, Sander C, Rätsch G, Caesar-Johnson SJ, Demchok JA, Felau I, Kasapi M, Ferguson ML, Hutter CM, Sofia HJ, Tarnuzzer R, Wang Z, Yang L, Zenklusen JC, Zhang JJ, Chudamani S, Liu J, Lolla L, Naresh R, Pihl T, Sun Q, Wan Y, Wu Y, Cho J, DeFreitas T, Frazer S, Gehlenborg N, Getz G, Heiman DI, Kim J, Lawrence MS, Lin P, Meier S, Noble MS, Saksena G, Voet D, Zhang H, Bernard B, Chambwe N, Dhankani V, Knijnenburg T, Kramer R, Leinonen K, Cancer Genome Atlas Research Network, et al. 2018. Comprehensive analysis of alternative splicing across tumors from 8,705 patients. Cancer Cell 34:211–224.e6.
15. Dvinge H, Kim E, Abdel-Wahab O, Bradley RK. 2016. RNA splicing factors as oncoproteins and tumour suppressors. Nat Rev Cancer 16:413–430. https://doi.org/10.1038/nrc.2016.51.
16. Sebestyén E, Singh B, Miñana B, Pagès A, Mateo F, Pujana MA, Valcárcel J, Eyras E. 2016. Large-scale analysis of genome and transcriptome alterations in multiple tumors unveils novel cancer-relevant splicing networks. Genome Res 26:732–744. https://doi.org/10.1101/gr.199935.115.
17. Conboy JG. 2017. Developmental regulation of RNA processing by Rbfox proteins. Wires Rna 8:e1398. https://doi.org/10.1002/wrna.1398.
18. Huh GS, Hynes RO. 1994. Regulation of alternative pre-mRNA splicing by a novel repeated hexanucleotide element. Genes Dev 8:1561–1574. https://doi.org/10.1101/gad.8.13.1561.
19. Jin Y, Suzuki H, Maegawa S, Endo H, Sugano S, Hashimoto K, Yasuda K, Inoue K. 2003. A vertebrate RNA-binding protein Fox-1 regulates tissue-specific splicing via the pentanucleotide GCAUG. EMBO J 22:905–912. https://doi.org/10.1093/emboj/cdg089.
20. Kuroyanagi H. 2009. Fox-1 family of RNA-binding proteins. Cell Mol Life Sci 66:3895–3907. https://doi.org/10.1007/s00018-009-0120-5.
21. Nakahata S, Kawamoto S. 2005. Tissue-dependent isoforms of mammalian Fox-1 homologs are associated with tissue-specific splicing activities. Nucleic Acids Res 33:2078–2089. https://doi.org/10.1093/nar/gki338.
22. Underwood JG, Boutz PL, Dougherty JD, Stoilov P, Black DL. 2005. Homologues of the *Caenorhabditis elegans* Fox-1 protein are neuronal splicing regulators in mammals. Mol Cell Biol 25:10005–10016. https://doi.org/10.1128/MCB.25.22.10005-10016.2005.
23. Zhang C, Zhang Z, Castle J, Sun S, Johnson J, Krainer AR, Zhang MQ. 2008. Defining the regulatory network of the tissue-specific splicing factors Fox-1 and Fox-2. Genes Dev 22:2550–2563. https://doi.org/10.1101/gad.1703108.
24. Ge X, Yamamoto S, Tsutsumi S, Midorikawa Y, Ihara S, Wang S, Aburatani H. 2005. Interpreting expression profiles of cancers by genome-wide survey of breadth of expression in normal tissues. Genomics 86:127–141. https://doi.org/10.1016/j.ygeno.2005.04.008.
25. Lapuk A, Marr H, Jakkula L, Pedro H, Bhattacharya S, Purdom E, Hu Z, Simpson K, Pachter L, Durinck S, Wang N, Parvin B, Fontenay G, Speed T, Garbe J, Stampfer M, Bayandorian H, Dorton S, Clark TA, Schweitzer A, Wyrobek A, Feiler H, Spellman P, Conboy J, Gray JW. 2010. Exon-level microarray analyses identify alternative splicing programs in breast cancer. Mol Cancer Res 8:961–974. https://doi.org/10.1158/1541-7786.MCR-09-0528.
26. Venables JP, Klinck R, Koh C, Gervais-Bird J, Bramard A, Inkel L, Durand M, Couture S, Froehlich U, Lapointe E, Lucier J-F, Thibault P, Rancourt C, Tremblay K, Prinos P, Chabot B, Elela SA. 2009. Cancer-associated regulation of alternative splicing. Nat Struct Mol Biol 16:670–676. https://doi.org/10.1038/nsmb.1608.
27. Braeutigam C, Rago L, Rolke A, Waldmeier L, Christofori G, Winter J. 2014. The RNA-binding protein Rbfox2: an essential regulator of EMT-driven alternative splicing and a mediator of cellular invasion. Oncogene 33:1082–1092. https://doi.org/10.1038/onc.2013.50.
28. Shapiro IM, Cheng AW, Flytzanis NC, Balsamo M, Condeelis JS, Oktay MH, Burge CB, Gertler FB. 2011. An EMT-driven alternative splicing program occurs in human breast cancer and modulates cellular phenotype. PLoS Genet 7:e1002218. https://doi.org/10.1371/journal.pgen.1002218.
29. Venables JP, Brosseau J-P, Gadea G, Klinck R, Prinos P, Beaulieu J-F, Lapointe E, Durand M, Thibault P, Tremblay K, Rousset F, Tazi J, Abou Elela S, Chabot B. 2013. RBFOX2 is an important regulator of mesenchymal tissue-specific splicing in both normal and cancer tissues. Mol Cell Biol 33:396–405. https://doi.org/10.1128/MCB.01174-12.
30. Quentmeier H, Icgc M-SC, Pommerenke C, Bernhart SH, Dirks WG, Hauer V, Hoffmann S, Nagel S, Siebert R, Uphoff CC, Zaborski M, Drexler HG, ICGC MMML-Seq Consortium. 2018. RBFOX2 and alternative splicing in B-cell lymphoma. Blood Cancer J 8. https://doi.org/10.1038/s41408-018-0114-3.
31. Van Nostrand EL, Pratt GA, Yee BA, Wheeler EC, Blue SM, Mueller J, Park SS, Garcia KE, Gelboin-Burkhart C, Nguyen TB, Rabano I, Stanton R, Sundararaman B, Wang R, Fu X-D, Graveley BR, Yeo GW. 2020. Principles of RNA processing from analysis of enhanced CLIP maps for 150 RNA binding proteins. Genome Biol 21. https://doi.org/10.1186/s13059-020-01982-9.
32. Kalsotra A, Xiao X, Ward AJ, Castle JC, Johnson JM, Burge CB, Cooper TA. 2008. A postnatal switch of CELF and MBNL proteins reprograms alternative splicing in the developing heart. Proc Natl Acad Sci U S A 105:20333–20338. https://doi.org/10.1073/pnas.0809045105.
33. Yeo GW, Coufal NG, Liang TY, Peng GE, Fu X-D, Gage FH. 2009. An RNA code for the FOX2 splicing regulator revealed by mapping RNA-protein interactions in stem cells. Nat Struct Mol Biol 16:130–137. https://doi.org/10.1038/nsmb.1545.
34. Chan Y-Y, Kalpana S, Chang W-C, Chang W-C, Chen B-K. 2013. Expression of aryl hydrocarbon receptor nuclear translocator enhances cisplatin

resistance by upregulating MDR1 expression in cancer cells. Mol Pharmacol 84:591–602. https://doi.org/10.1124/mol.113.087197.
35. Liang Y, Li W-W, Yang B-W, Tao Z-H, Sun H-C, Wang L, Xia J-L, Qin L-X, Tang Z-Y, Fan J, Wu W-Z. 2012. Aryl hydrocarbon receptor nuclear translocator is associated with tumor growth and progression of hepatocellular carcinoma. Int J Cancer 130:1745–1754. https://doi.org/10.1002/ijc.26166.
36. Barash Y, Calarco JA, Gao W, Pan Q, Wang X, Shai O, Blencowe BJ, Frey BJ. 2010. Deciphering the splicing code. Nature 465:53–59. https://doi.org/10.1038/nature09000.
37. Schultz A-S, Preussner M, Bunse M, Karni R, Heyd F. 2017. Activation-dependent TRAF3 exon 8 alternative splicing is controlled by CELF2 and hnRNP C binding to an upstream intronic element. Mol Cell Biol 37. https://doi.org/10.1128/MCB.00488-16.
38. Lovci MT, Ghanem D, Marr H, Arnold J, Gee S, Parra M, Liang TY, Stark TJ, Gehman LT, Hoon S, Massirer KB, Pratt GA, Black DL, Gray JW, Conboy JG, Yeo GW. 2013. Rbfox proteins regulate alternative mRNA splicing through evolutionarily conserved RNA bridges. Nat Struct Mol Biol 20:1434–1442. https://doi.org/10.1038/nsmb.2699.
39. Verma SK, Deshmukh V, Nutter CA, Jaworski E, Jin W, Wadhwa L, Abata J, Ricci M, Lincoln J, Martin JF, Yeo GW, Kuyumcu-Martinez MN. 2016. Rbfox2 function in RNA metabolism is impaired in hypoplastic left heart syndrome patient hearts. Sci Rep 6:30896. https://doi.org/10.1038/srep30896.
40. Belanger K, Nutter CA, Li J, Tasnim S, Liu P, Yu P, Kuyumcu-Martinez MN. 2018. CELF1 contributes to aberrant alternative splicing patterns in the type 1 diabetic heart. Biochem Biophys Res Commun 503:3205–3211. https://doi.org/10.1016/j.bbrc.2018.08.126.